


Research Article

A Beam Steering Dielectric Resonator Antenna Designed Using Rogers RO4003C Material for S-Band Applications

**Manisha Kumari,¹ Tavanam Venkata Rao,² S. Arun Jayakar,³ D. Srinivas,⁴
Dola Gobinda Padhan,⁵ A. Kishore Reddy,⁶ P. Rahul Reddy,⁷ and Amanuel Diriba Tura ⁸**

¹Department of Electronics and Communication Engineering, Gokaraju Rangaraju Institute of Engineering and Technology, Hyderabad-500090, Telangana, India

²Department of Electronics and Communication Engineering, Sreenidhi Institute of Science and Technology, Hyderabad 501301, India

³Department of Electronics and Instrumentation Engineering, Bannari Amman Institute of Technology, Erode 638401, India

⁴School of Business, SR University, Warangal-506371, India

⁵Department of Electrical and Electronics Engineering, Gokaraju Rangaraju Institute of Engineering and Technology, Hyderabad-500090, Telangana, India

⁶Department of Electrical and Communication Engineering, Andhra Engineering College, Nellore 524322, Andhra Pradesh, India

⁷Department of Electronics and Communication Engineering, Geethanjali Institute of Science and Technology, Nellore-524137, Andhra Pradesh, India

⁸Faculty of Mechanical Engineering, Jimma Institute of Technology, Jimma University, Jimma, Ethiopia

Correspondence should be addressed to Amanuel Diriba Tura; diriba.amanuel@ju.edu.et

Received 1 September 2022; Accepted 23 September 2022; Published 10 October 2022

Academic Editor: Vijayananth Kavimani

Copyright © 2022 Manisha Kumari et al. This is an open access article distributed under the Creative Commons Attribution License, which permits unrestricted use, distribution, and reproduction in any medium, provided the original work is properly cited.

A pattern reconfigurable dielectric resonator antenna emitting at 3.1 GHz is presented in this study. The beam can be steered at 6 degrees, 8 degrees, 14 degrees, and 171 degrees. Three P-i-N diodes are employed in the slots of the ground plane to help steer the beam direction. By changing the state of the three diodes, five states can be obtained. The $TE_{01\delta}$ mode is excited using a differential feed technique. Differential feed helps in increasing the gain and reducing the size of the structure. The return loss of each state is less than -25 dB. The gain of the first state is 7.65 dBi, the second and fifth state's gain is 8.22 dBi, third and fourth state's gain is 10.6 dBi. This Antenna is designed using Rogers RO4003C material which has low Electrical gravity, low voltage, and high oxidation resistance that makes it appropriate for RF applications. The properties required for RF microwave circuits, matching networks, and controlled impedance transmission lines are present in the RO4003C material. Annealed copper is used for designing the ground plane and feedline which provides excellent conductivity. The antenna is fabricated using the chemical etching process which employs a positive photoresist that gives a higher resolution accuracy for the designed antenna. This process of fabrication has another advantage of inculcating structures from simpler to complex.

1. Introduction

With the advent of wireless communication, the demand for reconfigurable antennas is increasing. Reconfigurable antennas are advantageous as they are compact, economical, and versatile, and they may replace an antenna array or several antennas. Reconfigurability can be categorized into frequency, pattern, polarization, and bandwidth. Pattern

reconfiguration can be done by mechanical tuning or electrical tuning. A pattern-reconfigurable multidirectional microstrip antenna for wireless communication was studied [1]. Utilizing switchable directors, a pattern-reconfigurable dielectric resonator antenna is created [2]. A straightforward arc dipole-based planar beam steerable antenna is presented [3]. Pattern reconfigurability using spherical shaped dielectric patch operating on higher order mode is designed

[4]. An antenna having five switchable beams in the elevation plane was investigated for pattern reconfiguration [5]. A cylindrical dielectric resonator antenna with pattern-reconfigurable components was developed [6]. The investigation of a gain-enhanced, pattern-reconfigurable planar Yagi-Uda antenna on a coplanar construction was proposed [7]. Wideband antennas with a reversible broadside and end-fire patterns were studied [8]. A reconfigurable pattern is produced by utilizing H-shaped components [9]. Demonstration of a dielectric liquid-based reconfigurable antenna with adjustable radiation pattern and polarization was proposed [10]. A wideband gravitational ball lens-based dielectric resonator antenna for circular polarization was investigated [11].

Dielectric resonator antenna is advantageous over microstrip patch antenna in terms of efficient radiation, bandwidth enhancement, and lesser conductor loss. At microwave and millimeter-wave frequency, the surface waves dominate in the case of microstrip patch antenna which eventually deteriorates the antenna efficiency, whereas DRAs do not suffer from surface waves and hence are more suitable at a higher frequency. Dielectric resonators with relative permittivity of 100 and higher are used in applications such as oscillators and filters. The higher the permittivity, the more the fields are tightly bound inside the material.

To make dielectric resonators work as an antenna the relative permittivity has to be between 3 and 50. When the relative permittivity is decreased, the fields when excited by the RF signal can escape and radiate. The DRAs have a distinct property of having distinct modes which when excited create distinct radiation patterns. DRAs offer simple feeding techniques such as microstrip feed, coaxial cable, and coplanar waveguide. They may therefore be integrated with many planar techniques. By adjusting the location of the DRA with regard to the line, it is simple to modify the coupling between a DR and a planar transmission line. By carefully selecting resonator settings, a DRA antenna's working bandwidth may be adjusted throughout a broad range. For instance, by selecting the right resonator material's dielectric constant, the bandwidths of a DR antenna's lower order modes may be readily changed from a tiny percentage to 10% or more.

The frequency range in which the antenna's input VSWR is smaller than a certain number of S is known as the impedance bandwidth of an antenna. The relationship between the entire unloaded Q -factor Q of the resonator and the impedance bandwidth of a resonant antenna, which is perfectly matched to a transmission line at its "resonant frequency," is as follows:

$$BW = \frac{(S - 1)}{Q\sqrt{S}}. \quad (1)$$

In this paper, a differential feed is used to excite the fundamental $TE_{01\delta}$ mode. Differential feed helps in reducing the cross-polarization and increases the gain of the antenna. Three slots are etched in the ground plane in which three p-i-n diodes are inserted. Altered states (on/off) of diode results

in beam steering. This antenna's DR construction is straightforward, and its switching speed is quick. Various studies are done on material specifications and antenna band selections [12–22].

The material, Rogers RO4003C is used as the substrate which provides low electrical gravity, low voltage, and high oxidation resistance that makes it appropriate for RF applications. All of the RO4003C laminates available configurations, which use both 1080 and 1674 glass fabric types, adhere to the same laminate electrical performance criteria. While using the same production procedure as ordinary epoxy/glass laminates, RO4003C laminates offer tight control over the dielectric constant (D_k) and minimal loss at a quarter of the cost of traditional microwave laminates. There are no additional through-hole treatments or handling techniques necessary, in contrast to PTFE-based microwave materials. Materials in the RO4003C category are not UL 94 V-0 certified and are not brominated.

The ground plane and the feedline are designed using annealed copper metal for better conductivity. The antenna is fabricated using the chemical etching process which employs a positive photoresist that gives higher resolution accuracy for antenna and other RF circuits. This process of fabrication has another advantage of inculcating structures from simpler to complex.

1.1. Antenna Configuration and Material Specifications.

The schematic of the antenna structure is depicted in Figure 1. The structure consists of a DP, substrate 1, ground plane, substrate 2, and a feed. The dielectric constant of the cylindrical DP is $\epsilon_{rd} = 45$, the loss tangent is $\tan \delta = 1.9 \times 10^{-4}$, and the volume is $\pi \times r \times r \times h \text{ mm}^3$ (where r = radius and h = height of the patch). Both substrates 1 and 2 are Rogers RO4003C with $\epsilon_{rs} = 3.38$, size of $L \times L \text{ mm}^2$ (L = length of the substrate. The thickness of substrate 1 is 1.524 mm and substrate 2 is 0.813 mm with $\tan \delta$ of 0.0027 is chosen for the present design. The length and width of the two substrates and ground plane are $60 \times 60 \text{ mm}^2$. The radius of the dielectric patch is 20.6 mm. The height of substrate 1 is 1.524 and substrate 2 is 0.813 mm. The length of feedback 1 is 14.5 mm and feedback 2 is 31 mm. The gap between the slots in the ground plane is 2.15 mm and the length of the slot is 8.5 mm. The relative permittivity of both substrates is 3.38 and that of the dielectric patch is 45.

All of the RO4003C laminates available configurations, which use both 1080 and 1674 glass fabric types, adhere to the same laminate electrical performance criteria. While using the same production procedure as ordinary epoxy/glass laminates, RO4003C laminates offer tight control over the dielectric constant (D_k) and minimal loss at a quarter of the cost of traditional microwave laminates. There are no additional through-hole treatments or handling techniques necessary, in contrast to PTFE-based microwave materials. Materials in the RO4003C category are not UL 94 V-0 certified and are not brominated. Hydrocarbon ceramic laminates with the RO4000 brand name are intended to provide improved high-frequency performance and

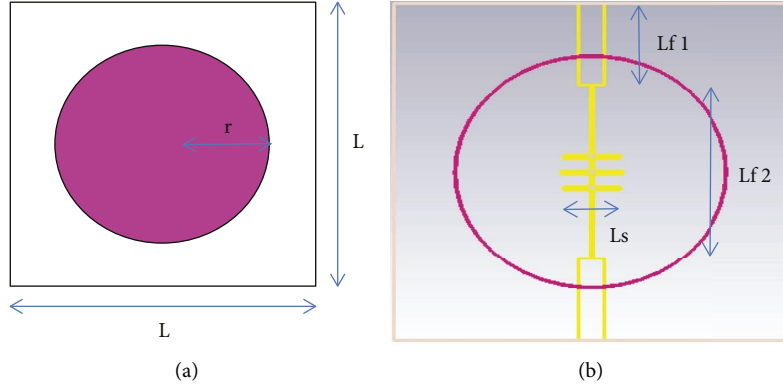


FIGURE 1: Schematic diagram of the pattern reconfigurable DP antenna. (a) The radius of the cylindrical DP. (b) Substrate along with feedline, diodes, and ground plane slots.

inexpensive circuit manufacturing. The outcome is a low-loss material that can be manufactured using common epoxy/glass (FR-4) techniques.

Once working frequencies reach 500 MHz and beyond, there are much less number of laminates to choose from. Higher operating frequencies prevent the use of traditional circuit board laminates in many applications, but reduced dielectric loss enables RO4000 series material to be utilized in such applications. Superior high-frequency performance and affordable circuit fabrication are two features of RO4000 hydrocarbon ceramic laminates. The properties required for RF microwave circuits, matching networks, and controlled impedance transmission lines are present in the RO4000 material. Figure 2 presents a variation of the relative permittivity of Rogers R04003C with temperature and frequency.

The Three connection slots are etched in parallel while the ground plane is positioned on the top layer of substrate 2. The area of slot 1 and slot 3 for simulation is $8.5 \times 0.9 \text{ mm}^2$, while slot 2 is $9.4 \times 0.6 \text{ mm}^2$. Three P-i-N diodes are kept in the coupling slots to provide the beam steering operation. The spacing, d , between the slots is 2.15 mm. The metal used for feedline and ground plane is annealed copper as they retain impact resistance to 20 K. Copper becomes flexible after being annealed. Annealing restores electrical conductivity by enhancing the crystal lattice's uniformity. The resistivity of annealed copper is $1.72 \times 10^{-8} \text{ ohm-m}$ and its specific gravity is 8.89. The modulus of elasticity is 17,000,000 psi. Table 1 presents the specifications of annealed copper and Figure 3 shows the variation of stress with respect to strain for annealed copper (Table 2).

1.2. Mathematical Analysis of TE_{mn} Mode. For the purpose of directing the ensuing design, a mathematical study of the TE_{mn} mode is necessary. The theoretical analytical model of the DP resonator is depicted in Figure 4 beneath.

As magnetic walls, four side planes that are perpendicular to the z -axis direction are considered. The resonator is half-cut by using the ground plane as an electric wall. In accordance with the Helmholtz equation and boundary conditions [23].

$$\begin{aligned} \nabla^2 \cdot E_z + k^2 \cdot E_z &= 0 \\ \nabla^2 \cdot H_z + k^2 \cdot H_z &= 0. \end{aligned} \quad (2)$$

It is possible to retrieve the TE_{mn} mode's field element expressions.

For the DP

$$\left(|z| \leq \frac{h_d}{2} \right) \quad (3)$$

$$H_{z1}(x, y, z) = A_1 \sin(k_x x) \sin(k_y y) \cos[k_z z + \varphi_z].$$

For air ($z > h_d/2$)

$$\begin{aligned} H_{z2}(x, y, z) &= A_1 \cos\left(\frac{k_z h_d}{2} + \varphi_z\right) \\ &\times \sin(k_x x) \sin(k_y y) e^{-\alpha_1 \left(z - \frac{h_d}{2}\right)}. \end{aligned} \quad (4)$$

For the substrate ($-h_d/2 - h_{s1} \leq z \leq -h_d/2$)

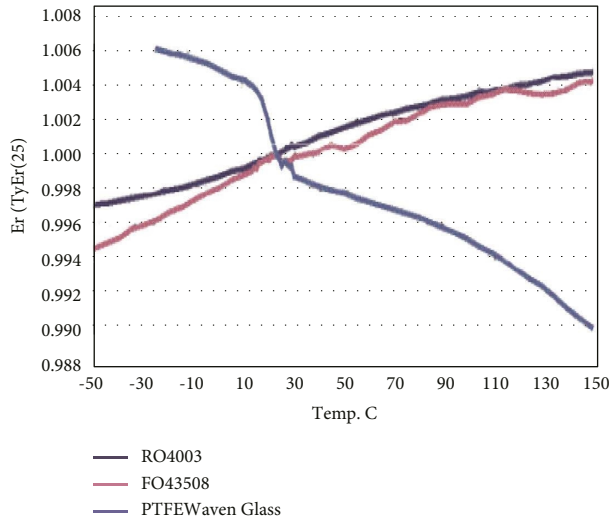
$$\begin{aligned} H_{z3}(x, y, z) &= \frac{A_1 \cos(k_z h_d/2 - \varphi_z)}{\sinh(\alpha_2 h_{s1})} \sin(k_x x) \sin(k_y y) \\ &\times \sinh\left[\alpha_2 \left(z + \frac{h_d}{2} + h_{s1}\right)\right]. \end{aligned} \quad (5)$$

The wave numbers of the z -axis dissipation mode in air and substrate, respectively, are represented in the aforementioned formulas by α_1 and α_2 , respectively. The wave numbers on the x , y , and z axes are denoted by the letters k_x , k_y , and k_z .

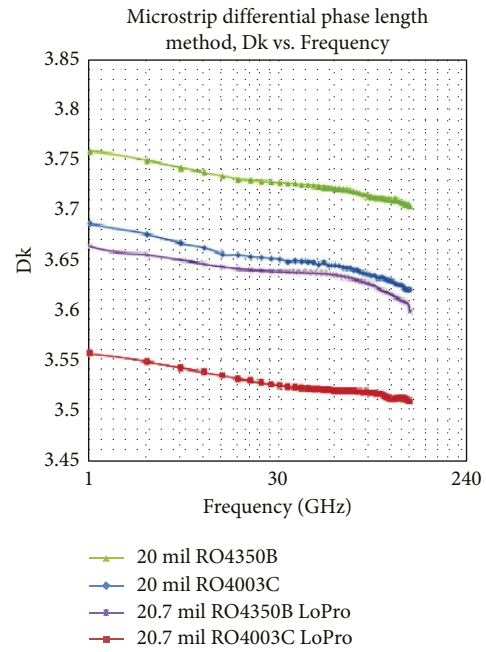
$$k_x = \frac{m\pi}{w_d}, \quad (6)$$

$$k_y = \frac{n\pi}{w_d}.$$

The following equations are used to obtain the remaining field components in the DP, air, and substrate.



(a)



(b)

FIGURE 2: Variation of RO4003C relative permittivity with (a) temperature and (b) frequency.

TABLE 1: Specification of annealed copper.

Specific gravity	8.89
Density	0.322 lb./cu. In. At 68°F
Thermal conductivity	226 BTU/Sq Ft/Ft/Hr°F at 68°F
Coefficient of thermal expansion	0.0000098/°F from 68°F to 572°F
Modulus of elasticity	17,000,000 psi
Tensile strength	32,000 psi min
Yield strength (0.5% extension)	20,000 psi min
Elongation in 2" approx	30%
Shear strength	25,000 psi
Hardness, rockwell	54 min

TABLE 2: Parameter dimensions.

Parameters	Dimension (mm)
L	60
R	20.6
$Lf1$	14.5
$Lf2$	31
Ls	8.5
$h1$	1.524
$h2$	0.813
D	2.15

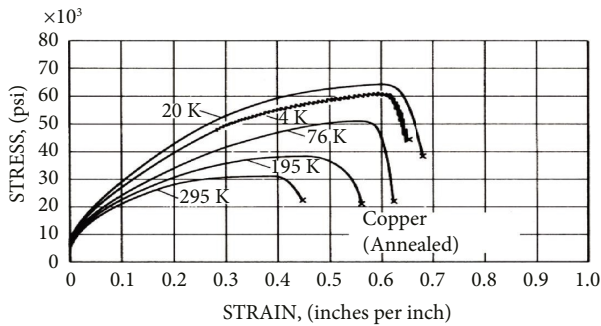


FIGURE 3: Stress vs strain variation of annealed copper.

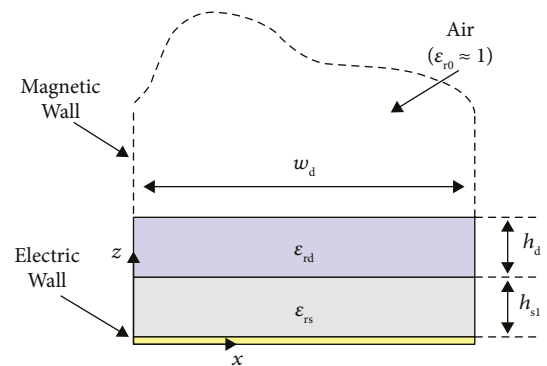


FIGURE 4: Modeling of DP resonator.

$$\begin{aligned}
E_x &= -\frac{j\omega\mu_0}{k_c^2} \frac{\partial H_z}{\partial x}, \\
E_y &= -\frac{j\omega\mu_0}{k_c^2} \frac{\partial H_z}{\partial x}, \\
H_x &= \frac{1}{k_c^2} \frac{\partial^2 H_z}{\partial x \partial z}, \\
H_y &= \frac{1}{k_c^2} \frac{\partial^2 H_z}{\partial y \partial z}.
\end{aligned} \tag{7}$$

The following formula is therefore derived in accordance with the continuous criterion for the tangential H-field and E-field at the DP interfaces:

$$\begin{aligned}
k_z \cdot h_d &= \tan^{-1} \left(\frac{\alpha_1}{k_z} \right) + \tan^{-1} \left(\frac{\alpha_2 \coth(\alpha_2 h_{s1})}{k_z} \right), \\
\varphi_z &= \frac{\tan^{-1}(\alpha_1/k_z) - \tan^{-1}(\alpha_2 \coth(\alpha_2 h_{s1})/k_z)}{2}.
\end{aligned} \tag{8}$$

Lastly, when paired with classical electromagnetism's preservation of wavelength range

$$\begin{aligned}
k_x^2 + k_y^2 + k_z^2 &= \epsilon_r \epsilon_0 k_0^2 \\
k_x^2 + k_y^2 - \alpha_1^2 &= \epsilon_{r0} k_0^2 \\
k_x^2 + k_y^2 - \alpha_2^2 &= \epsilon_{rs} k_0^2.
\end{aligned} \tag{9}$$

1.3. Reconfigurability Principle. Three coupling slots loaded with P-i-N diodes are placed in the ground plane to provide beam steering, as depicted in Figure 1. Five switching states that function at roughly 3.1 GHz can be accomplished by adjusting the ON-/OFF state of the P-i-N diodes, as listed in Table 3. BAR64-02V P-i-N diode is used whose equivalent diagram is shown in Figure 5. Conventional silicon fabrication techniques, such as oxidation, photolithography, ion implantation, aluminum sputter deposition, and passivation, were used to create the diodes. Boron was implanted into the bare wafer to create the diode's front side (p + active area). For an n + contact, the phosphorous was doped on the back side. State 1 is established when D_1 is ON and D_2 and D_3 are OFF. In this instance, as depicted in Figure 6, the E-field of the $TE_{01\delta}$ mode is evenly spread across the DP resonator.

The half-power beamwidth (HPBW) is 87.6 degrees, while the main beam orientation is 8 degrees. State 1 has a 7.65 dBi peak gain. State 2 has a primary beam direction of 14 degrees and an HPBW of 88.6 degrees when D_1 and D_2 are OFF and D_3 is ON. State 2 has an 8.22 dBi peak gain. State 3 is when just D_3 is OFF but D_1 and D_2 are ON. In this situation, the HPBW is 66.5 degrees, while the main beam direction is 171 degrees. 10.6 dBi is added to the peak gain. In the fourth condition, D_1 and D_3 are OFF while D_2 is ON, producing a gain of 10.6 dBi and a relatively high HPBW of 171 degrees in comparison with the other modes.

2. Results and Discussion

The E field distribution of $TE_{01\delta}$ mode at 3.1 GHz as shown in Figure 6 is derived by using the Eigenmode solver in CST Microwave studio. This $TE_{01\delta}$ mode generates a distinct radiation pattern that is broadside. A differential feed is given to the designed structure which results in higher gain. A differential feed excites the cylindrical DRA in such a way that $TE_{01\delta}$ mode is excited. For a differential feed to work, both the ports carry the same amplitude but 180 degrees out of phase Rf signal. The ON state of the P-i-N diode is given by providing a 2.1 ohm Resistor. The OFF state is a parallel RC circuit of $R=500$ Ohm and $C=2.1$ pF. A parametric analysis has been carried out in terms of the distance between the slots (d) for each state and state 2 by varying d from 0.15 to 2.15 mm. The return loss for state 1 and state 2 as shown in Figure 7 below can be read to be ranging from -25 dB to -32 dB for state 1. The return loss for state 2 with varying d ranges from -25 to -28 dB. A second parametric analysis was carried out with the radius (r) of the cylindrical DP. The radius varied from 10.6 mm to 20.6 mm showing a return loss ranging from -31 to -33 dB. Finally, the structure was optimized at $d=2.15$ mm and a radius, $r=20.6$ mm.

Figure 8 depicts return loss for different radius values of the dielectric patch. The designed structure provides a return loss of -28 dB and a wide bandwidth as can be seen in Figure 9. State 1 provides a return loss of -28 dB, while state 2 and state 4 provide a S11 Value of -30 dB. The return loss of state 3 is < -40 dB. The major lobe direction of state 1 is 8 degrees whereas that of state 2 is 14 degrees as shown in Figure 10. Figure 11 represents the 3D radiation plot of state 1, state 2, and state 3. States 1 and 2 have a broadside radiation pattern. The gain of state 1 is 7.65 dBi, while that of state 3 and state 4 is 10.6 dBi. State 2 and state 5 provide a gain of 8.22 dBi. A comparison of different techniques of pattern reconfiguration using the switching method has been carried out in Table 4. [1] A microstrip patch antenna is studied which consists of 6 switches and 6 states at 3.7 GHz with a gain of 6 dBi. A DRA [4] is investigated with 3 switches comprising of 3 states at 5.8 GHz providing a gain of 7.48 dBi. An MPA with 20 switches and 5 states operating at 2.4 GHz providing a gain of 6.5 dBi is studied [5]. With an increase in the number of switches, the loss increases, and it makes the structure bulkier. [8] An MPA with 8 switches and 9 states resonating at 2.5 GHz with a gain of 7.26 dBi is investigated. [11] presents an MPA with 17 switches and only 3 states radiating at 3.5 GHz and providing a gain of 9 dBi. A DRA [24] with 8 switches and 8 states operating at 5.8 GHz with a gain of 7.27 dBi is studied. The present antenna structure provides better efficiency compared to the other structures in terms of the implementation of the number of diodes and the maximum number of states attainable. The gain as compared to previous structures is also higher which makes it suitable for indoor wireless communication. Many researchers have used various techniques to engineer the devices along with suitable antennas to accommodate for better performance [25–34].

TABLE 3: Switching states of the proposed antenna.

State	D1	D2	D3	S11 (dB)	Gain (dBi)	Beam direction	HPBW	Side lobe (dB)
1	ON	OFF	OFF	-28	7.65	8°	87.6°	-5
2	OFF	ON	OFF	-37	8.22	14°	88.6°	-2.7
3	ON	ON	OFF	-30	10.6	171°	66.5°	-2
4	OFF	ON	ON	-30	10.6	-171°	171°	-2
5	OFF	OFF	ON	-30	8.22	6°	83.3°	-4.7

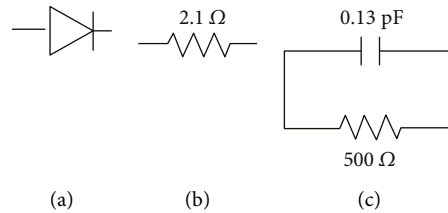


FIGURE 5: (a) P-i-N diode; (b) on state; (c) off state.

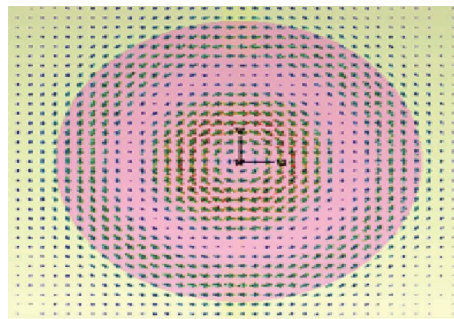


FIGURE 6: E field distribution of $TE_{01\delta}$ mode at 3.1 GHz.

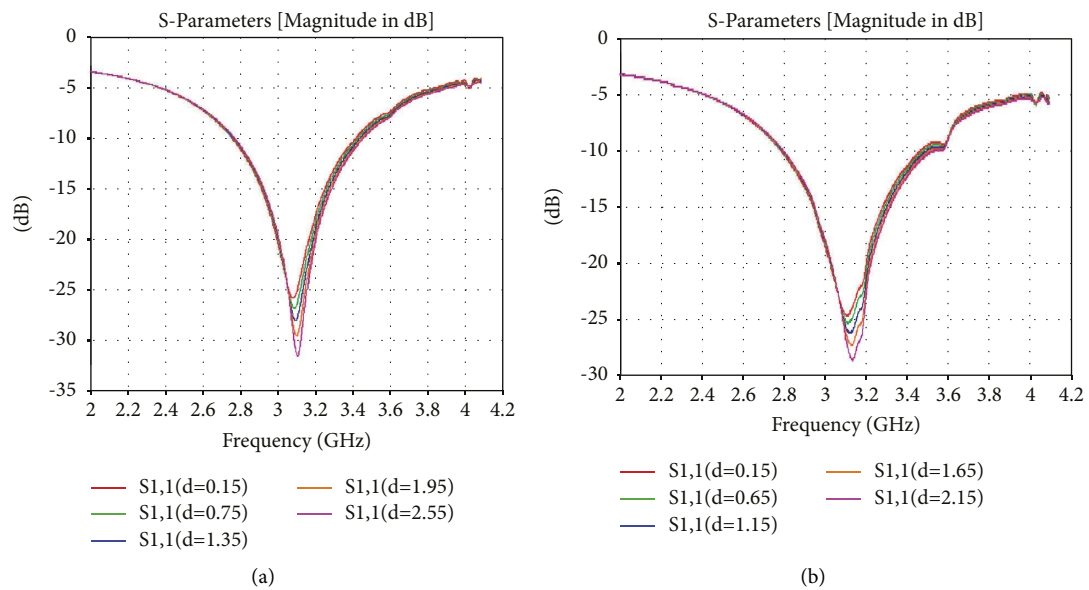


FIGURE 7: Parametric analysis of the distance between the slots of (a) state 1 and (b) state 2.

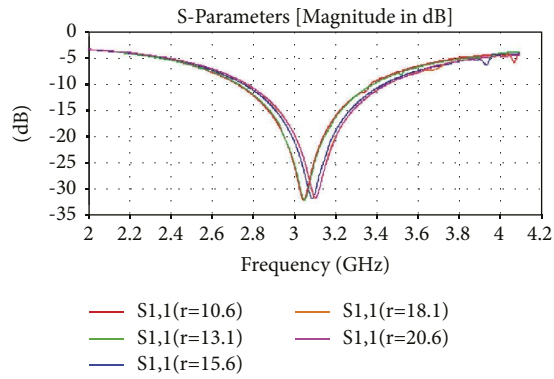


FIGURE 8: Parametric analysis of the return loss for different radius values of the dielectric patch.

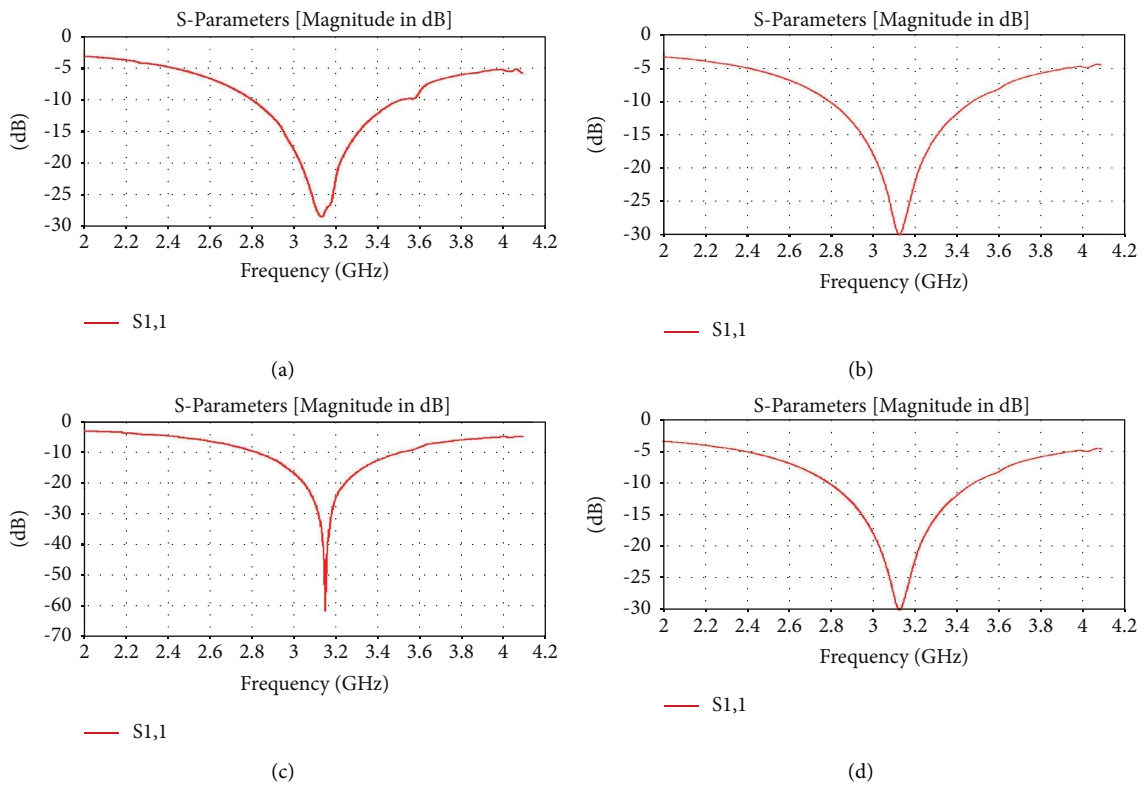


FIGURE 9: Return loss of (a) state 1, (b) state 2, (c) state 3, and (d) state 4.

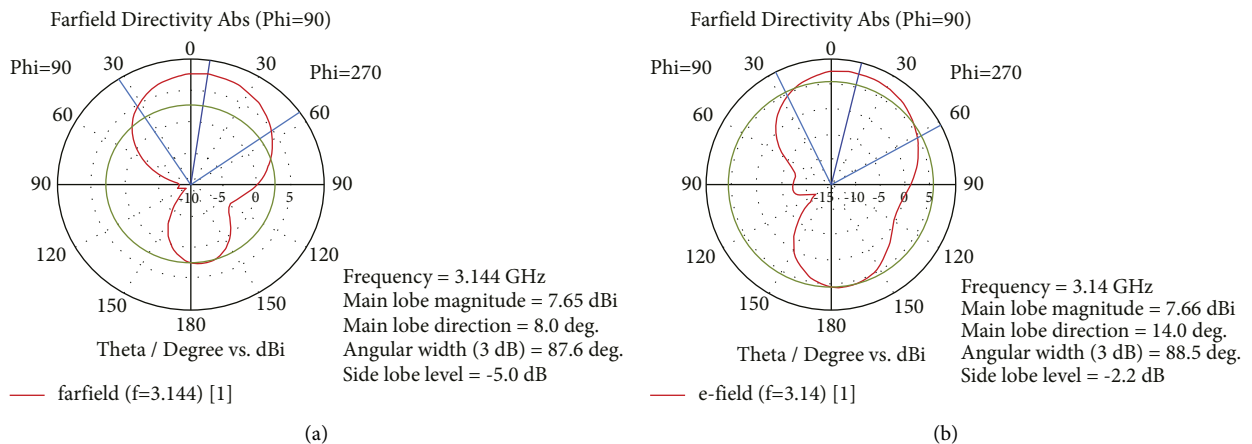


FIGURE 10: Polar plot of (a) state 1 and (b) state 2.

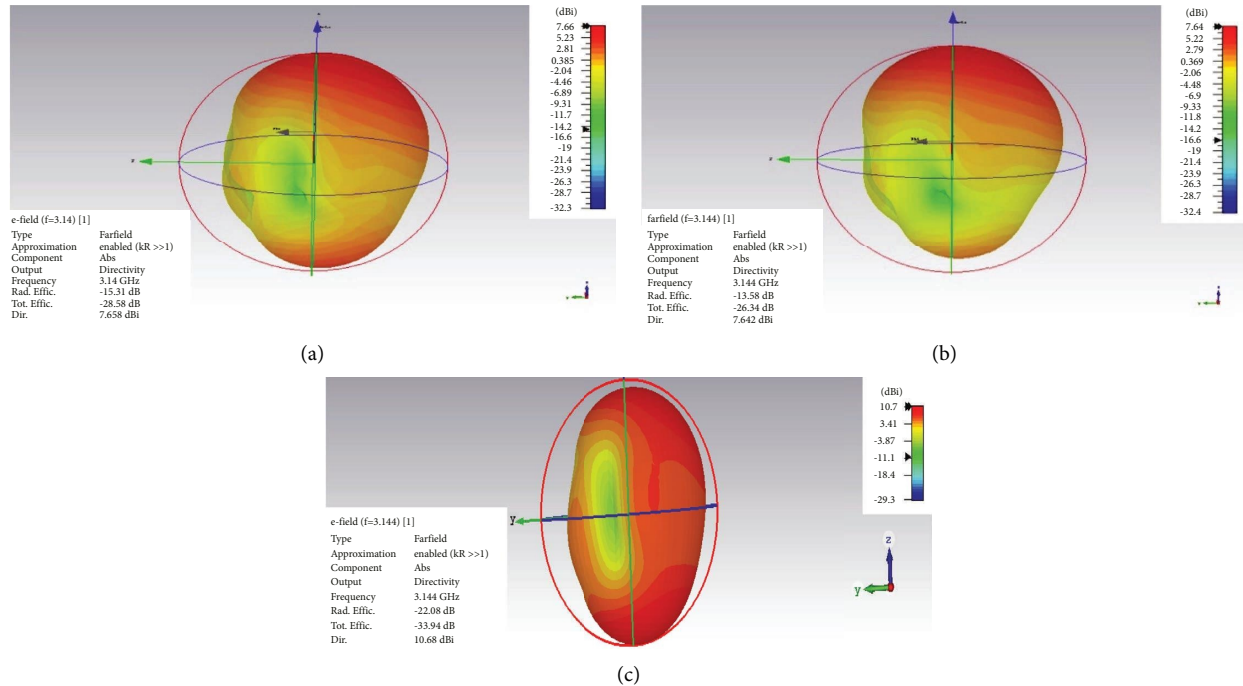


FIGURE 11: 3D radiation pattern of (a) state 1, (b) state 2 and (c) state 3.

TABLE 4: Comparison of different pattern reconfiguration techniques.

Reference	Antenna type	Number of switches	Number of states	F0 (GHz)	Gain (dBi)
[1]	MPA	6	6	3.7	6
[4]	DRA	3	3	5.8	7.48
[5]	MPA	20	5	2.4	6.5
[8]	MPA	8	9	2.5	7.26
[10]	MPA	8	4	3.4	7.3
[11]	MPA	17	3	3.5	9
[24]	DRA	8	8	5.8	7.27
Present work	DRA	3	5	3.1	10.6

3. Fabrication Process

An appropriate material must be prepared before the process of fabrication. Both the electrical requirements for antenna applications and the requirements for deep lithography manufacturing should be met by the material. Permittivity and dielectric loss are two crucial electrical properties of the material. Direct/indirect manufacturing techniques may be thought of to create effective and feasible antenna structures depending on the material qualities. The direct procedure prioritizes lithography fabrication suitability; as a result, pure photoresist materials with/without a minimal amount of additives are acceptable.

The indirect technique relies heavily on the material's electrical qualities, allowing for the use of significant amounts of non-photoresist materials with superior electrical capabilities. Direct manufacturing is simpler and easier than indirect fabrication, which involves first creating a high-aspect-ratio photoresist frame before utilizing a robotic machine to inject microwave material into the frame. Here the substrate used is Rogers RO4003C having a relative

permittivity of 3.38 and $\tan\delta = 0.0027$. Organic polymers used as photoresist materials undergo chemical changes when exposed to UV light. The photoresist is positive when the exposed region becomes more soluble in the developer. If it becomes less soluble, the substance is regarded as a negative resist. The exposed areas of negative resists increase as the developer dissolves the counterpart, which impairs the process's ability to resolve itself.

The developer solution seeps into the photoresist material, causing swelling, which in turn causes a distortion in the patterned area.

As a result, positive resists are being used more frequently than negative ones in photolithography-based antenna fabrication because they offer superior resolution.

4. Conclusion

A pattern reconfigurable dielectric resonator antenna emitting at 3.1 GHz is presented in this paper. The beam can be steered at 6 degrees, 8 degrees, 14 degrees, and 171 degrees. Three P-i-n diodes are employed in the slots of the

ground plane to help steer the beam direction. By changing the state of the three diodes, five states can be obtained. The return loss of each state is less than -25 dB. The gain of the first state is 7.65 dBi, the second and fifth state's gain is 8.22 dBi, and the third and fourth state's gain is 10.6 dBi. A differential feed excites the $TE_{01\delta}$ mode, reduces the design complexity, makes it low profile, and enhances the gain. A mathematical analysis of TE_{mn} is elaborated which forms the basis for understanding the working of the antenna. The E field of the excited $TE_{01\delta}$ is presented which in turn generates a broadside radiation pattern. The Antenna can be a good contender for S-band applications. The structure is designed using Rogers RO4003C which offers higher longevity, Low electrical gravity, low voltage, and high oxidation resistance making it useful in RF applications including airplane and media domains. The relative permittivity of the substrate (Rogers RO4003C) is 3.38 with $\tan\delta = 0.0027$. They are low-loss materials that can be produced using common epoxy/glass (FR-4) fabrication techniques that are reasonably priced. Once operational frequencies reach 500 MHz and above, the range of laminates typically available is significantly constrained. The properties of RF microwave circuits, matching networks, and controlled impedance transmission lines are present in the RO4000 material. Annealed copper is used to design the ground plane and feedline which provides excellent conductivity. The Antenna is fabricated using the chemical etching process which employs a positive photoresist that inculcates structures from simpler to complex while giving a higher resolution accuracy for the designed Antenna. [35–41]

Data Availability

The data used to support this study are included within the article.

Ethical Approval

This article does not contain any studies with human or animal subjects.

Conflicts of Interest

The authors declare that they have no conflicts of interest regarding the publication of this paper.

Acknowledgments

The authors are thankful to Jimma Institute of Technology, Jimma University, Jimma, Ethiopia for their cooperation and support during this research work. The publication of this research work is only for the academic purpose of Jimma University, Ethiopia.

References

- [1] G. Yang, J. Li, D. Wei, S.-G. Zhou, and R. Xu, "Pattern reconfigurable microstrip antenna with multidirectional beam for wireless communication," *IEEE Transactions on Antennas and Propagation*, vol. 67, no. 3, pp. 1910–1915, 2019.
- [2] Y. H. Ke, L.-L. Yang, and J.-X. Chen, "A pattern-reconfigurable dielectric resonator antenna based on switchable Directors," *IEEE Antennas and Wireless Propagation Letters*, vol. 21, no. 3, pp. 536–540, 2022.
- [3] G. Jin, M. Li, D. Liu, and G. Zeng, "A simple planar pattern-reconfigurable antenna based on arc dipoles," *IEEE Antennas and Wireless Propagation Letters*, vol. 17, no. 9, pp. 1664–1668, 2018.
- [4] B. K. Ahn, H.-W. Jo, J.-S. Yoo, J.-W. Yu, and H. L. Lee, "Pattern reconfigurable high gain spherical dielectric resonator antenna operating on higher order mode," *IEEE Antennas and Wireless Propagation Letters*, vol. 18, no. 1, pp. 128–132, 2019.
- [5] S.-L. Chen, P.-Y. Qin, W. Lin, and Y. J. Guo, "Pattern-reconfigurable antenna with five switchable beams in elevation plane," *IEEE Antennas and Wireless Propagation Letters*, vol. 17, no. 3, pp. 454–457, 2018.
- [6] B.-J. Liu, J.-H. Qiu, C.-L. Wang, and G.-Q. Li, "Pattern-reconfigurable cylindrical dielectric resonator antenna based on parasitic elements," *IEEE Access*, vol. 5, Article ID 25584, 2017.
- [7] S. Raman, N. Timmons, and J. Morrison, "Gain enhanced pattern reconfigurable planar Yagi-Uda antenna on coplanar structure," *Electronics Letters*, vol. 49, no. 25, pp. 1593–1595, 2013.
- [8] X. Ding and B.-Z. Wang, "A novel wideband antenna with reconfigurable broadside and endfire patterns," *IEEE Antennas and Wireless Propagation Letters*, vol. 12, pp. 995–998, 2013.
- [9] J. Ren, X. Yang, J. Yin, and Y. Yin, "A novel antenna with reconfigurable patterns using H-shaped structures," *IEEE Antennas and Wireless Propagation Letters*, vol. 14, pp. 915–918, 2015.
- [10] J. Ren, Z. Zhou, Z. H. Wei et al., "Radiation pattern and polarization reconfigurable antenna using dielectric liquid," *IEEE Transactions on Antennas and Propagation*, vol. 68, no. 12, pp. 8174–8179, 2020.
- [11] Z. Chen, Q. Liu, B. Sanz-Izquierdo, H. Liu, J. Yu, and X. Chen, "A wideband circular-polarized beam steering dielectric resonator antenna using gravitational ball lens," *IEEE Transactions on Antennas and Propagation*, vol. 69, no. 5, pp. 2963–2968, 2021.
- [12] R. Deepa, M. P. Devi, N. A. Vignesh, and S. Kanithan, "Implementation and performance evaluation of ferroelectric negative capacitance FET," *Silicon*, vol. 14, no. 5, pp. 2409–2419, 2022.
- [13] E. S. Kumar, S. Kumar P, N. Arun Vignesh, and S. Kanithan, "Design and analysis of junctionless FinFET with Gaussian doped for non-polar structure," *Silicon*, vol. 14, pp. 8439–8447, 2022.
- [14] S. Kanithan, N. ArunVignesh, E. Karthikeyan, and N. Kumaresan, "An intelligent energy efficient cooperative MIMO-AF multi-hop and relay based communications for Unmanned Aerial Vehicular networks," *Journal of Computer and Communications*, vol. 154, pp. 254–261, 2020.
- [15] R. Senthil, G. M. Tamil selvan, S. Kanithan, and N. Arun Vignesh, "Routing in WSNs powered by a hybrid energy storage system through a CEAR protocol based on cost welfare and route score metric," *International Journal of Computers, Communications & Control*, vol. 14, no. 2, pp. 233–252, 2019.
- [16] B. Shilpa, L. K. Rao, N. A. Vignesh, and V. V. Kumar, "Design of inset fed circular dual band patch antenna for WLAN

- frequencies,” *International Journal of Systems, Control and Communications*, vol. 13, no. 1, pp. 56–66, 2022.
- [17] N. Arun Vignesh and P. Poongodi, “Analysis of localized quality of service improvement architecture for wireless LAN,” *Wireless Personal Communications*, vol. 90, no. 2, pp. 701–711, 2016.
- [18] N. A. Vignesh and P. Poongodi, “A cluster-based network architecture scheme for QoS improvement in WLAN,” *International Journal of Networking and Virtual Organisations*, vol. 17, no. 2/3, pp. 158–169, 2017.
- [19] S. Kanithan, A. Ananthanarayanan, N. Arun Vignesh, and T. Kannapiran, “Improved imperialist competitive algorithm based energy efficient peak to average power ratio (papr) in cooperative mimo-of systems,” in *Proceedings of the International Conference on Computer Communication and Informatics (ICCCI)*, pp. 1–5, Coimbatore, India, January 2022.
- [20] K. Murali, N. A. Vignesh, S. Kanithan, N. Kumaresan, P. Vidyullatha, and D. V. Babu, “Two stage signal processing of channel valuation and recognition for millimeter MIMO systems,” in *Proceedings of the International Conference on Computer Communication and Informatics (ICCCI) Coimbatore, India*, pp. 1–5, January 2022.
- [21] N. S. Kiran, N. A. Vignesh, S. Kanithan et al., “Cross coupled power effective quick level shifter,” in *Proceedings of the International Conference on Computer Communication and Informatics (ICCCI) Coimbatore, India*, pp. 1–5, January 2022.
- [22] L. G. N. S. Pratyusha, K. Keerthi, K. S. Reddy, and E. S. Sushma, “A study on wideband spectrum monitoring using NI USRP,” in *Proceedings of the International Conference on Computer Communication and Informatics (ICCCI) Coimbatore, India*, pp. 1–4, January 2022.
- [23] K. M. Luk and K. W. Leung, *Dielectric Resonator Antennas, “Research Studies”*, Press Ltd, Hertfordshire, England, UK, 2003.
- [24] L. Zhong, J.-S. Hong, and H.-C. Zhou, “A novel pattern-reconfigurable cylindrical dielectric resonator antenna with enhanced gain,” *IEEE Antennas and Wireless Propagation Letters*, vol. 15, pp. 1253–1256, 2016.
- [25] S. S. P. Tammireddy, M. Samson, P. R. Reddy et al., “An energy-efficient reconfigurable accelerators in multi-core systems using PULP-NN,” *Applied Nanoscience*, vol. 21, pp. 1–14, 2021.
- [26] A. L. Narayana, B. Prasad, P. R. Kapula, D. Prasad, A. K. Panigrahy, and D. N. V. S. L. S. Indira, “Enhancement in performance of DHT precoding over WHT for EC companded OFDM in wireless networks,” *Applied Nanoscience*, pp. 1–16, 2021.
- [27] M. D. Prakash, B. G. Nelam, S. Ahmadsaidulu, A. Navaneetha, and A. K. Panigrahy, “Performance analysis of ion-sensitive field effect transistor with various oxide materials for biomedical applications,” pp. 1–11, Silicon, 2021.
- [28] M. D. Prakash, S. L. Nihal, S. Ahmadsaidulu, R. Swain, and A. K. Panigrahy, “Design and modelling of highly sensitive glucose biosensor for Lab-on-chip applications,” pp. 1–7, Silicon, 2022.
- [29] A. Kumar Panigrahi and K.-N. Chen, “Low temperature Cu-Cu bonding Technology in 3D integration: an extensive review,” *Journal of Electronic Packaging*, vol. 140, no. 1, Article ID 010801, 2018.
- [30] A. K. Panigrahy, T. Ghosh, S. R. K. Vanjari, and S. G. Singh, “Surface density gradient engineering precedes enhanced diffusion; drives CMOS in-line process flow compatible Cu-Cu thermocompression bonding at 75° C,” *IEEE Transactions on Device and Materials Reliability*, vol. 19, no. 4, pp. 791–795, 2019.
- [31] N. A. Vignesh, R. Kumar, R. Rajarajan et al., “Silicon wearable body area antenna for speech-enhanced IoT and nanomedical applications,” *Journal of Nanomaterials*, vol. 2022, Article ID 2842861, 9 pages, 2022.
- [32] A. K. Panigrahi, T. Ghosh, S. R. K. Vanjari, and S. G. Singh, “Oxidation resistive, CMOS compatible copper-based alloy ultrathin films as a superior passivation mechanism for achieving 150 C Cu-Cu wafer on wafer thermocompression bonding,” *IEEE Transactions on Electron Devices*, vol. 64, no. 3, pp. 1239–1245, 2017.
- [33] S. Bonam, A. K. Panigrahi, C. H. Kumar, S. R. K. Vanjari, and S. G. Singh, “Interface and reliability analysis of Au-passivated Cu-Cu fine-pitch thermocompression bonding for 3-D IC applications,” *IEEE Transactions on Components, Packaging, and Manufacturing Technology*, vol. 9, no. 7, pp. 1227–1234, 2019.
- [34] A. K. Panigrahi, T. Ghosh, C. H. Kumar, S. G. Singh, and S. R. K. Vanjari, “Direct, CMOS in-line process flow compatible, sub 100° C Cu-Cu thermocompression bonding using stress engineering,” *Electronic Materials Letters*, vol. 14, no. 3, pp. 328–335, 2018.
- [35] C. Song, E. L. Bennett, J. Xiao et al., “Passive beam-steering gravitational liquid antennas,” *IEEE Transactions on Antennas and Propagation*, vol. 68, no. 4, pp. 3207–3212, 2020.
- [36] B. Li and K. W. Leung, “On the differentially fed rectangular dielectric resonator antenna,” *IEEE Transactions on Antennas and Propagation*, vol. 56, no. 2, pp. 353–359, 2008.
- [37] Z.-L. Lu, X.-X. Yang, and G.-N. Tan, “A multidirectional pattern reconfigurable patch antenna with CSRR on the ground,” *IEEE Antennas and Wireless Propagation Letters*, vol. 16, pp. 416–419, 2017.
- [38] W.-Q. Deng, X.-S. Yang, C.-S. Shen, J. Zhao, and B.-Z. Wang, “A dual polarized pattern reconfigurable Yagi patch antenna for microbase stations,” *IEEE Transactions on Antennas and Propagation*, vol. 65, no. 10, pp. 5095–5102, 2017.
- [39] M. A. Towfiq, A. Khalat, S. Blanch, J. Romeu, L. Jofre, and B. A. Cetiner, “Error vector magnitude, intermodulation, and radiation characteristics of a bandwidth- and pattern-reconfigurable antenna,” *IEEE Antennas and Wireless Propagation Letters*, vol. 18, no. 10, pp. 1956–1960, 2019.
- [40] R. L. Haupt and M. Lanagan, “Reconfigurable antennas,” *IEEE Antennas and Propagation Magazine*, vol. 55, no. 1, pp. 49–61, 2013.
- [41] J. Costantine, Y. Tawk, S. E. Barbin, and C. G. Christodoulou, “Reconfigurable antennas: design and applications,” *Proceedings of the IEEE*, vol. 103, no. 3, pp. 424–437, 2015.